# Friction and Adhesion Govern Yielding of Disordered Nanoparticle Packings: A Multiscale Adhesive Discrete Element Method Study

Xiaohui Liu<sup>1,2,3,†</sup>, Joel A. Lefever<sup>4,§,†</sup>, Daeyeon Lee<sup>5</sup>, Jie Zhang<sup>6,7</sup>, Robert W. Carpick<sup>8,\*</sup>, Ju Li<sup>3,9,\*</sup>

<sup>1</sup>Institute of Materials Modification and Modeling, School of Materials Science and Engineering, Shanghai Jiao Tong University, Shanghai 200240, China

<sup>2</sup>Materials Genome Initiative Center, Shanghai Jiao Tong University, Shanghai 200240, China
<sup>3</sup>Department of Nuclear Science and Engineering, Massachusetts Institute of Technology, Cambridge, MA 02139, USA

<sup>4</sup>Department of Materials Science and Engineering, University of Pennsylvania, Philadelphia, PA 19104, USA <sup>5</sup>Department of Chemical and Biomolecular Engineering, University of Pennsylvania, Philadelphia, PA 19104, USA <sup>6</sup>Institute of Natural Sciences, Shanghai Jiao Tong University, Shanghai 200240, China

<sup>7</sup>School of Physics and Astronomy, Shanghai Jiao Tong University, Shanghai 200240, China
<sup>8</sup>Department of Mechanical Engineering and Applied Mechanics, University of Pennsylvania, Philadelphia, PA
19104. USA

<sup>9</sup>Department of Materials Science and Engineering, Massachusetts Institute of Technology, Cambridge, MA 02139, USA

§Current Affiliation: Asylum Research — an Oxford Instruments Company, Santa Barbara, CA 93117, USA †X. Liu and J. Lefever contributed equally

\*To whom correspondence should be addressed: <u>carpick@seas.upenn.edu</u> (R. Carpick) or <u>liju@mit.edu</u> (J. Li)

## **ABSTRACT**

Recent studies have demonstrated that amorphous materials, from granular packings to atomic glasses, share multiple striking similarities, including a universal onset strain level for yield. This is despite vast differences in length scales and in the constituent particles' interactions. However, the nature of localized particle rearrangements is not well understood, and how local interactions affect overall performance remains unknown. Here, we introduce a multiscale adhesive discrete element method to simulate recent novel experiments of disordered nanoparticle packings indented and imaged with single nanoparticle resolution. The simulations exhibit multiple behaviors matching the experiments. By directly monitoring spatial rearrangements, and interparticle bonding/de-bonding under the packing's surface, we uncover the mechanisms of the yielding and hardening phenomena observed in experiments. Interparticle friction and adhesion synergistically toughen the packings and retard plastic deformation. Moreover, plasticity can result from bond switching without particle rearrangements. These results furnish insights for understanding yielding in amorphous materials generally.

**Keywords**: Amorphous material, granular matter, discrete element simulation, nanoindentation, localized rearrangements, softness

#### I. INTRODUCTION

The plasticity and flow of many classes of disordered packings have been investigated by experiments and simulations, including granular packings (typically with grains > 1  $\mu$ m) such as sand<sup>1-3</sup>, pillars<sup>4-6</sup> and disks<sup>7,8</sup>, and those composed of smaller-scale constituents, including disordered nanoparticle packings (DNPs)<sup>9-13</sup>. Studies have demonstrated that disordered packings across many size scales exhibit similar physics<sup>14</sup>, such as localized constituent particle rearrangements<sup>4</sup>, shear banding<sup>10</sup>, and brittle fracture<sup>13</sup>. Similar phenomena are also observed in many other amorphous materials, including metallic glasses<sup>15-19</sup> and colloidal glasses<sup>20,21</sup>. Despite these advances, the nature of these localized constituent-level rearrangements is still a rapidly developing area<sup>22</sup>, with many unanswered questions.

Interparticle friction is a prominent aspect of granular materials, which sets them apart from bubble rafts<sup>23</sup> and slowly deformed colloids<sup>20</sup>, and yields specific phenomena such as random loose packing<sup>24</sup>, shear jamming<sup>25,26</sup>, and anomalous diffusion<sup>1,2</sup>. Friction should affect the performance of DNPs as well<sup>11</sup>, though with nanoscopic friction laws that are possibly different from macroscopic laws<sup>27,28</sup>. It is of both scientific and engineering significance to investigate the effect of friction on the properties of disordered packings at various length scales. However, it is challenging in experiments to alter friction and thereby tune the resulting properties.

For grain sizes below ca. 1 µm, it is also essential to address how interparticle adhesion affects the disordered packing's mechanical performance. This is because many DNPs with appealing functionality<sup>29-37</sup> have found only limited application owing to their poor mechanical reliability and durability<sup>10,38</sup>, wherein interparticle adhesion plays a critical role. While adhesion is known to impact certain aspects in adhesive disordered packings, such as the jamming phase diagram<sup>39</sup>, critical phenomena<sup>40</sup>, and the packing fraction<sup>41-43</sup>, to date limited consideration has been given to how adhesion affects the mechanical response to external stimuli.

Among amorphous materials, DNPs are unique in that both friction and adhesion could be significant, making DNPs appropriate to serve as model materials to compare with other disordered systems, including granular matter and atomic glasses. In prior research, we investigated the plastic deformation of silica DNPs using atomic force microscopy (AFM)-based single-particle indentation<sup>11</sup>. Using high-resolution imaging and tracking, we succeeded in reproducibly indenting on top of a *single* chosen nanoparticle in the packing. This stands in

contrast to conventional nanoindentation experiments, where resolution at the individual particle level (i.e., atoms or molecules) is not achievable. It thus permitted us to: (1) study the yielding of a disordered packing whose constituent particles are considered as "artificial atoms", i.e., as proxies for atoms in an amorphous material; the results validated that the behavior could be generalized and applied to understanding mechanisms of mechanical failure for disordered materials; and (2) learn about the behavior of these specific nanoparticle packings, whose application relevance is discussed above. From this, we argued that the results bear on amorphous material behavior in general. Specifically, we confirmed that yielding begins with localized rearrangements at the scale of a few particle diameters. This matches the proposed universal correlation lengthscale for rearrangement sizes observed on several disordered materials<sup>14</sup>.

However, the AFM method is not able to resolve particles located in the packing's interior, being restricted to imaging particles at the packing's surface. Thus, the underlying mechanisms of the mechanical responses could not be fully explored by the experiment itself.

Subsequently, we altered interparticle interactions by introducing water vapor into the system, leading to the formation of liquid bridges between nanoparticles via capillary condensation<sup>12</sup>. Nevertheless, it is difficult to quantitatively determine how capillary bridges affect adhesion forces at this nanometer length scale. Therefore, this method is not a perfect analog for tuning adhesion. In general, it is challenging to directly vary adhesion between the constituents of a disordered material experimentally, although some recent notable studies with granular<sup>6</sup> and colloidal<sup>44</sup> particles have succeeded in doing so.

Inspired by the unique experiments described above <sup>11,12</sup>, here we develop a novel multiscale adhesive discrete element method (MADEM) to simulate silica DNPs under single nanoparticle-level indentation. The MADEM simulations enable full resolution of each nanoparticle's position, with complete tunability of interparticle friction and adhesion along with many other desired parameters, which is challenging or impossible to accomplish experimentally. This allows exploration of how these factors modulate the packings' mechanical performance, and provides insights potentially applicable to other disordered systems.

We demonstrate that there is strong heterogeneity in the particle-scale mechanical responses for the DNPs, with force-chain like heterogeneous structures similar to those of macroscopic granular materials, except that both friction and adhesion are crucial. We find that the interparticle normal contact and sliding frictional bonding and de-bonding play critical roles in governing yielding and hardening in the DNPs, even in the absence of particle rearrangements. This is a new paradigm for considering the nature of the unit processes involved in the plasticity of disordered materials. We also find a strong synergy between interparticle friction and adhesion in stabilizing and toughening the DNPs, which is not achieved in frictionless or nearly adhesionless packings.

#### II. METHODOLOGY

The traditional discrete element method (DEM)<sup>45</sup> has been extensively applied to investigate granular material behavior. To apply DEM to DNP simulations, one must introduce interparticle adhesion. In MADEM, we describe the normal elastic interaction between deformable particles with adhesion via a multiscale adhesive contact model<sup>46</sup>, in which elastic contact is modelled within the framework of continuum mechanics involving large deformation, while interparticle adhesion is formulated by coarse-graining the interaction of molecules with neighboring particles using an intermolecular potential. This contact model is implemented within a nonlinear finite element formulation to simulate full-range contact processes between a spherical particle and a rigid plane to generate interparticle potentials with various effective radii. Based on these, we then develop a robust, efficient on-the-fly interpolation scheme to extract the adhesive normal contact force between particles with arbitrary effective radii, since our packings are polydisperse. Three other common modes of particle interaction due to friction – sliding, twisting, and rolling – are also incorporated in MADEM following previous work<sup>47-50</sup>. MADEM is implemented in the LAMMPS code<sup>51</sup>; detailed methodology is found in Sec. I in Supporting Information (SI).

To match the characteristics of the previously investigated alumina-coated silica DNPs<sup>11</sup>, 4000 particles with a uniform diameter distribution within 20.0±4.8 nm are randomly generated within a box. In such a system, gravity may be ignored. The particles' elastic properties are taken to be those of amorphous silica, while the adhesion interaction is chosen to match the alumina coating. The default work of adhesion  $w_0$  from van der Waals interactions between particles is obtained using the computed Hamaker constant of  $\alpha$ -alumina<sup>52</sup> (See Sec. II in SI for consideration of error introduced here). Some other types of interactions, like covalent or hydrogen bonding, could also be present in the experiments<sup>11</sup>. Thus, we vary the adhesion strength by boosting the work of adhesion w to be multiples of  $w_0$  (See Sec. III in SI for the sample preparation details). The packing fraction of the silica DNPs obtained is close to or above the random close packing limit<sup>24</sup> depending on w (Sec. IV in SI).

Table 1 lists the key parameters used in the MADEM indentation simulations. The indenter is modeled as a sphere with mechanical properties matching that of diamond to mimic the spherical tip of the hard, tetrahedral amorphous carbon AFM probe used in experiments<sup>11</sup>. The effects of the indenter size and the indentation velocity on the indentation load are presented in Secs. V and VI in SI, respectively. We also tune the sliding friction coefficient  $\mu_s$  and work of adhesion w between particles to investigate their effects on the DNP's mechanical response, as discussed below.

Table 1. Key parameters for the MADEM indentation simulations. The default values are used in all simulations except for those where that parameter is tuned.

Parameter	Default value	Range investigated	Reference
Number of particles	4000	N/A	N/A
Particle diameter	20.0±4.8 nm	Polydisperse but not varied	(11)
Packing size	$\approx 370 \times 370 \times 200 \text{ nm}^3$	Slightly varied depending on w	Chosen to diminish the effect of the packing size
Indenter radius	8 nm	6–16.7 nm	(11)
Indentation velocity	0.1 m/s	0.01-1 m/s	Limited by simulation timescale
Sliding friction coefficient ( $\mu_s$ )	0.3	0-0.6	(28)
Work of adhesion (w)	109.62 mJ/m <sup>2</sup> (w <sub>0</sub> )	$(0-11)\times w_0$	(52)

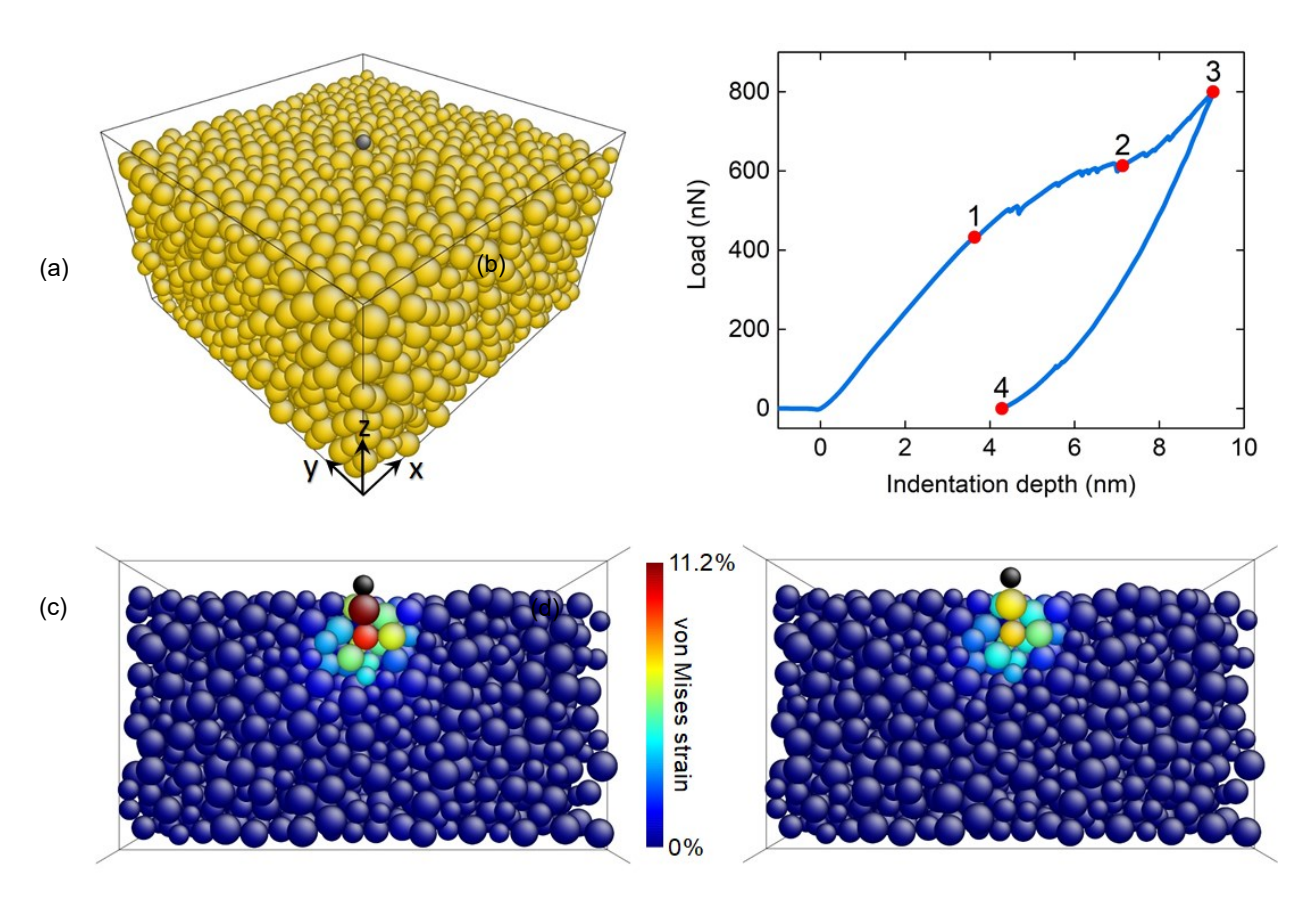


Figure 1. (a) Schematics of the configuration of a DNP for single-particle indentation simulation. (b) A typical simulated indentation load curve with  $\mu_s = 0.3$ ,  $w = 7w_0$  and the maximum load of 800 nN. (c) A cross-sectional view of the configuration at the maximum load corresponding to point 3 labeled in (b). (d) Configuration at the end of the indentation corresponding to point 4 labeled in (b). The size of the packing is about  $370\times370\times200$  nm<sup>3</sup>, with periodic boundary conditions in the *x* and *y* directions, a silicon substrate on the bottom, and a free surface on the top. The black sphere denotes the indenter, with a radius of 8 nm. The particles are colored by their affine von Mises strain defined in Ref. (53) as measured relative to their initial positions, visualized by AtomEye<sup>54</sup>. See Supporting Movie S1 for the full evolution of the packing configuration over the course of indentation.

## III. RESULTS AND DISCUSSION

A typical simulated indentation load curve and the packing configurations illustrating the deformation under the applied load are shown in Fig. 1 and Supporting Movie S1. Following the experiments<sup>11</sup>, the simulation is run until a load of 800 nN is reached, and then the indenter is withdrawn. The strain remaining after the indentation demonstrates that plastic deformation has

occurred. The majority of plastic deformation is limited to a region a few particles in size beneath the indenter, and there is almost no strain near the lateral boundaries and the substrate over the course of indentation, implying a fairly weak boundary effect.

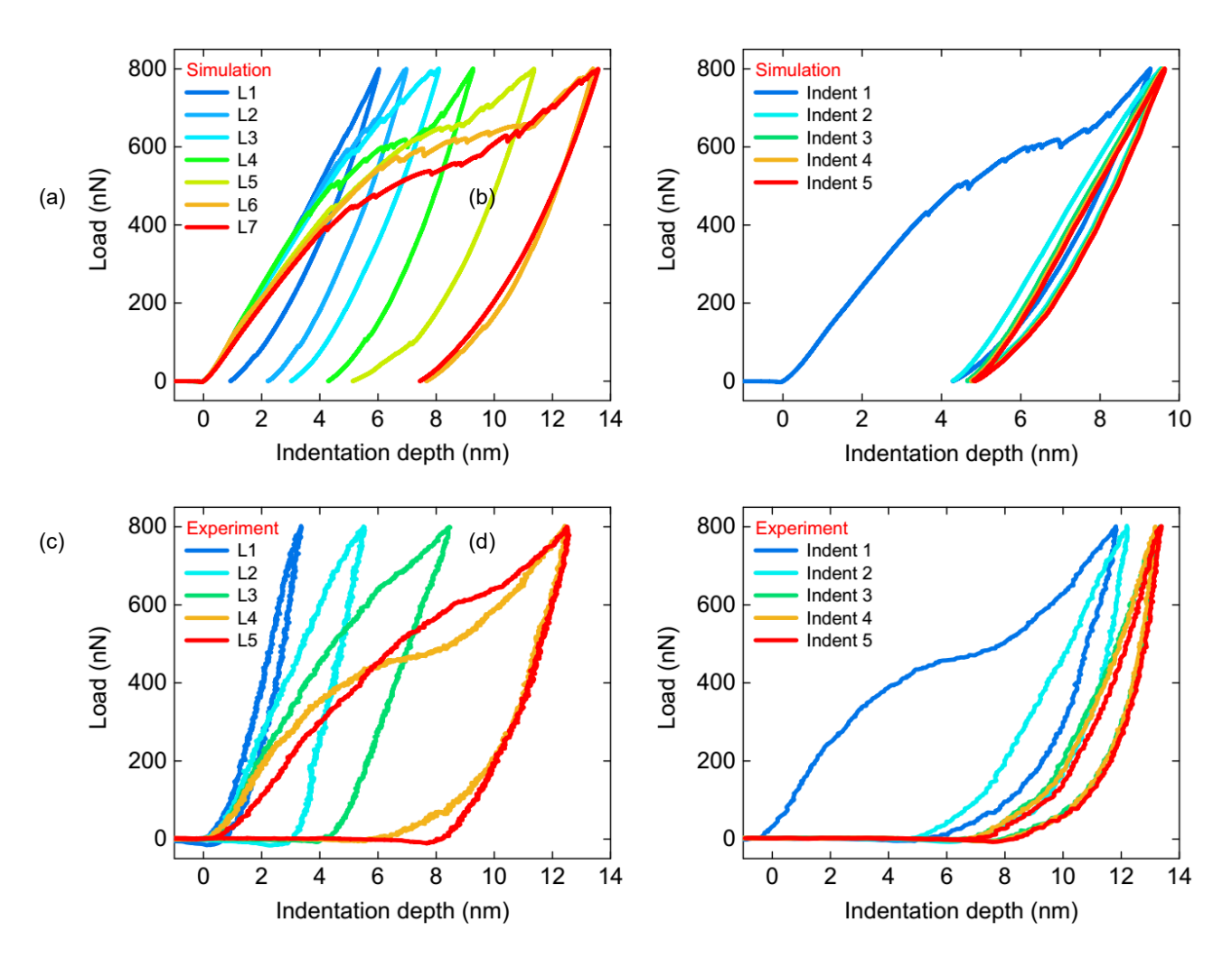


Figure 2. (a) Simulated load curves for seven different locations indented on the packing given in Fig. 1. (b) Simulated load curves of a series of five repeated indents performed at a single location on the packing. For comparison, Figs. 5a and 5b from Ref. (11) are reproduced as (c) and (d) here, showing the experimental results of the load curves for different locations and for repeated indents at a single location, respectively. All the curves have the maximum load of 800 nN. Note that the samples used in the simulations are not guaranteed to have particles with the same position and size as those used in the experiments, since we lack the information about the particles within the interior of the latter due to the limitation of AFM.

Multiple specific phenomena from experiments are reproduced well. Fig. 2a shows the load curves resulting from indentation simulations performed at various locations on the DNP film. Substantial differences are apparent including a large variation in the indentation depth, indicating that the local mechanical properties vary spatially across the film. Deeper indents correspond to greater energy dissipation. Specifically, load curves corresponding to deeper indentation depths also enclose a larger area with a greater residual indentation depth after unloading, implying a locally soft region is where more plastic deformation occurs and not simply more elastic compliance. Fig. 2b shows simulated load curves obtained by repeated indentation at the same location. The hysteresis in each curve indicates that energy is lost due to dissipative mechanisms, which are explained further below. These results compare favorably with Fig. 5 of Ref. (11) (as reproduced by Figs. 2c and 2d here), particularly regarding the indentation depths and elastic moduli. For instance, we observe a similar range of indentation depths at randomly selected locations, in the range of 6.0–13.6 nm in simulations (Fig. 2a), and 3.4–12.5 nm in experiments (Fig. 2c). Also, the substantial plastic deformation on the initial indent followed by nearly pure elastic deformation in subsequent indents (Fig. 2b), closely matches the previous experimental results (Fig. 2d).

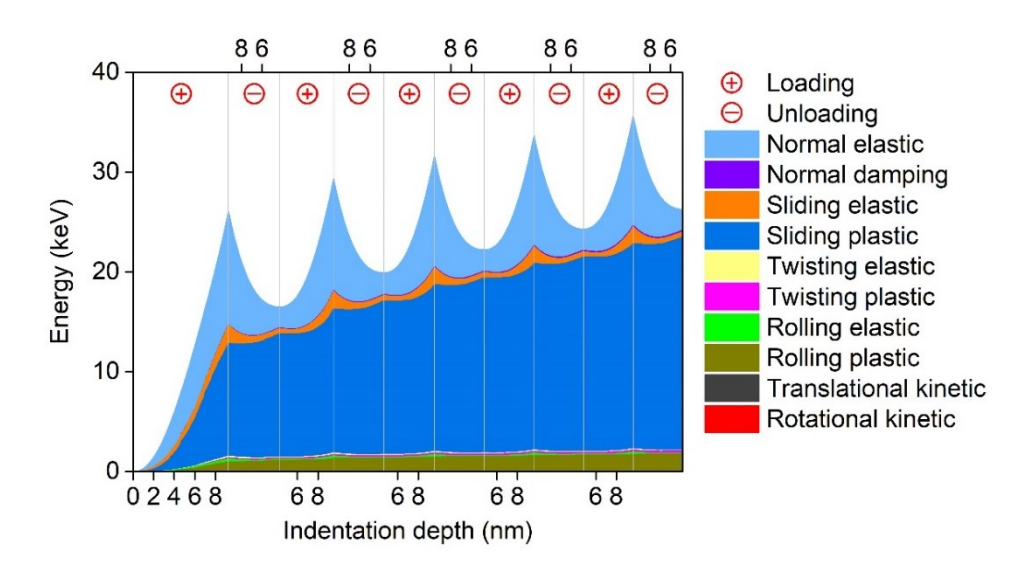


Figure 3. Evolution of the energy accumulated and dissipated in the packing over the course of five complete indent cycles repeated at the same location, corresponding to Fig. 2b. The sliding/twisting/rolling elastic energy denotes the energy stored elastically owing to static friction between particles, while the sliding/twisting/rolling plastic energy denotes that dissipated owing to kinetic friction between particles. The formulas for the energy calculation are listed in Table S3 in SI.

Simulation results demonstrate that the most significant form of energy dissipation is the sliding friction between the particles, in both the first indent cycle and the subsequent cycles in Fig. 2b, as shown in Fig. 3. In addition to the dissipated plastic energy, some energy is also stored elastically in the form of adhesive normal contact strain and sliding/twisting/rolling elastic strains at particle interfaces. Not all the elastic energy is recovered when the load is withdrawn due to strain energy stored in these interparticle bonds. Kinetic energy accounts for only a small portion of the total energy, supporting the treatment of DNP indentation as a quasi-static process. Similar to the previous experiments<sup>11</sup>, the characteristic energy magnitude is on the order of tens of keV, which is mainly shared among tens of particles positioned locally beneath the indenter. This demonstrates that our packing system can be treated as athermal. In this regard, thermal activation, which is usually omitted in granular matter, should play a negligible role as well in our DNPs.

In prior experiments<sup>11</sup>, an inflection is frequently observed in the indentation load curves with deep indents, as shown in Figs. 2c (L4 and L5) and 2d (Indent 1). This indicates that the packing undergoes plastic yielding and hardening before and after the inflection. However, the mechanisms of the yielding and hardening remained elusive because the AFM cannot explore the packing's interior. Our simulations reproduce these phenomena well (Figs. 2a and 2b), enabling us to peer into the configurational evolution and analyze the interparticle interactions. Fig. 4 shows the local topologies under the indenter as well as the truss-like normal contact force chains and the sliding frictional force chains corresponding to the timepoints 1–3 labeled in Fig. 1b, which correspond to before initial yielding, after initial yielding (at the inflection point), and within the hardening stage, respectively. Since only particle 1 bridges the indenter (labeled as particle 0), its motion, due to the interactions with all its neighbors, immediately influences the indentation load. Surface particles 2–6 impose most of the frictional resistance to particle 1 along the z direction (Fig. 4b), while particles 8 and 9, which are the closest sub-surface particles to particle 1, carry much of the normal force to balance particle 1 from below (Fig. 4a). Before yielding, particles 2 and 3 exert attractive forces on particle 8 as a result of adhesion (Fig. 4a-1), but these two bonds are broken afterward (Fig. 4a-2) as particle 8 is constantly driven by particle 1 from above. Moreover, particle 8 is further attracted by particles 14 and 15 from below by forming new bonding. Almost simultaneously, particle 9 loses the bond with attractive force from particle 5. These drive particles 8 and 9 to accelerate to move downwards with conspicuous z-displacements, as shown in Fig. 4a-2, which relaxes the repulsive force acting on particle 1. This change of the force chains greatly

affects the trajectory of particle 1 thereafter and also the load transmitted to the indenter, then followed by yielding. The above analysis demonstrates that the plastic deformation is the result of bond switching without significant local rearrangements below the indenter. This bond switching phenomenon is frequently observed in our simulations and is seen explicitly in Supporting Movie S2.

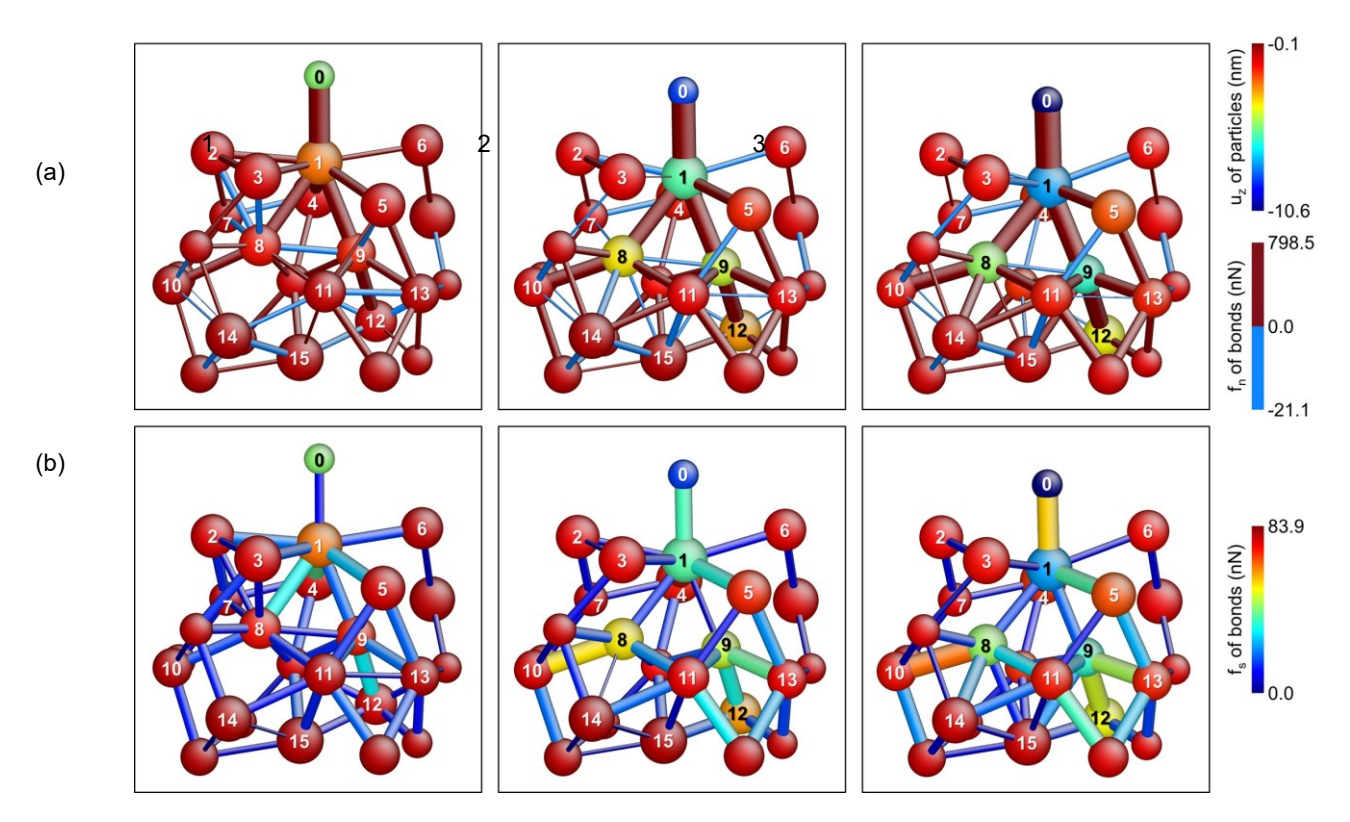


Figure 4. Snapshots of the local configuration under the indenter with the numerical labels 1-3 on the top corresponding to the points labeled in Fig. 1b. The indenter is labeled as 0. (a) The bonds display the interparticle normal contact force  $(f_n)$  chains, with repulsive (positive) and attractive (negative)  $f_n$  colored by red and blue, respectively. This binary color scheme is chosen to make the bonds with repulsion and attraction more distinguishable. (b) Here, the bonds display the sliding frictional force  $(f_s)$  chains, colored according to the magnitude of  $f_s$ . In (a) and (b), the bond size reflects the magnitude of the respective interparticle force, with the bond radii scaled proportional to  $|f_n|^{1/3}$  (or  $|f_s|^{1/2}$ ) rather than  $|f_n|$  (or  $|f_s|$ ) in order to make the bonds with small  $|f_n|$  (or  $|f_s|$ ) more visible. The particles themselves are colored by their z-displacement  $u_z$ , and have been scaled down to make the bonds visible. See Supporting Movie S2 for the full evolution of the  $f_n$  and  $f_s$  chains over the course of indentation. Detailed conditions for the formation and breakage of the bonds can be found in Sec. I in SI.

The hardening mechanism can also be revealed by analysis of the bonding evolution. Under further indentation, particle 9 gains stronger support from particle 12, and the normal contact forces of the bonds 8-14 and 8-15 change from attraction to repulsion, which contributes to supporting particle 8 from below. In the meantime, as shown in Fig. 4b, particle 8 is subjected to stronger frictional forces by its neighboring particles 10, 11 and 14, as does particle 9 by particles 11 and 13. These particles resist the downward motion of particle 1 and the indenter, which is responsible for the ensuing hardening. In experiments<sup>11</sup>, the larger AFM tip had more chance to collide with the surface particles, which could also contribute to the hardening and has been validated by our simulations (see Sec. V in SI). These two hardening mechanisms above can be differentiated by using a smaller indenter as in our simulations.

The effects of friction and adhesion on the mechanical response of the DNPs under indentation are investigated by either changing  $\mu_s$  or w, as shown in Fig. 5. The structural stability of the DNPs is remarkably improved by the introduction of both friction and adhesion (Figs. 5a and 5b) as compared to the nearly adhesionless (Fig. 5c) and frictionless (Fig. 5d) systems. Furthermore, increasing either  $\mu_s$  (Fig. 5a) or w (Fig. 5b) can enhance the loading stiffness of the packings in the presence of both friction and adhesion, though the underlying mechanisms are different in these two cases. The projection of the frictional tangential forces in the normal direction can compensate for the normal contact forces between particles and prevent the breaking of contacts<sup>55</sup>, thus making the packings stiffer. In contrast, stronger adhesion yields shorter equilibrium interparticle separations naturally, which brings about a higher elastic modulus of the packings as well. With regard to unloading, friction plays a much less important role, especially in the early stage of retraction, as evidenced by the drastic drop of the sliding plastic power dissipation shown in Fig. S12 in SI. Accordingly, unloading largely reflects the intrinsic elasticity of the packing, which is quite dependent on the adhesion strength. This can explain why the initial unloading stiffness, which determines the indentation modulus  $^{56}$ , is fairly sensitive to the change of w (Fig. 5b) but not to  $\mu_s$  except for very small  $\mu_s$  (Fig. 5a). Another observation from Figs. 5a and 5b is that either friction or adhesion can delay the onset of yielding, signifying a higher energy barrier to be surmounted for plastic deformation. However, plastic deformation cannot be eliminated even if we greatly increase  $\mu_s$  or w. This indicates that the local plasticity or softness is decided by both the local structure and energetics<sup>57,58</sup>.

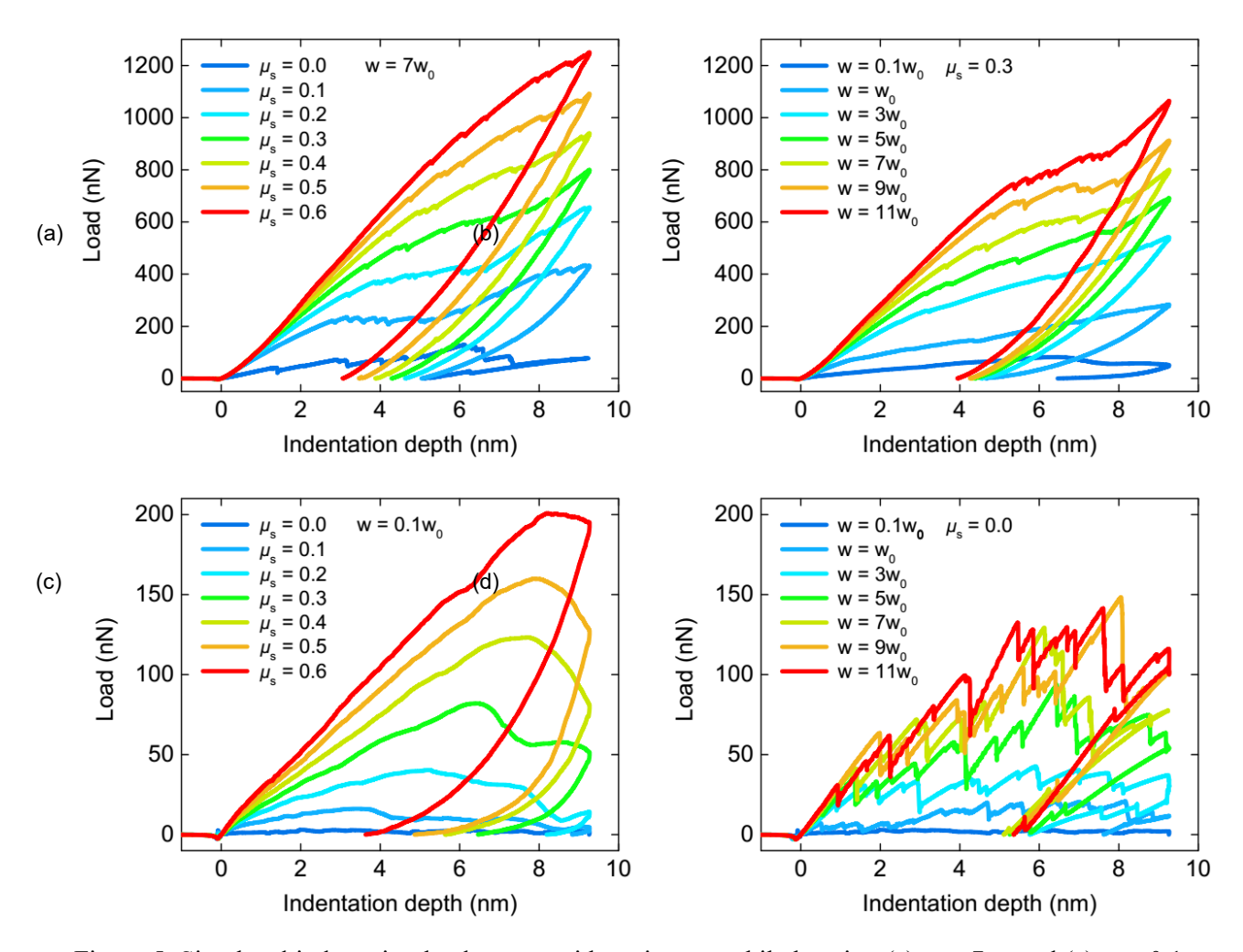


Figure 5. Simulated indentation load curves with various  $\mu_s$  while keeping (a)  $w = 7w_0$  and (c)  $w = 0.1w_0$ , and with various w while keeping (b)  $\mu_s = 0.3$  and (d)  $\mu_s = 0$ . We choose to investigate the packings with weak adhesion in (c) instead of purely adhesionless ones (w = 0), as the latter lose their original marginal rigidity states and disassemble under the perturbation by indentation. All the simulations in (a) and (c) are performed using the same initial packing configuration and at the same indent location, respectively. The initial packing configurations with different w used in (b) and (d) share a certain similarity in topology, respectively (see Sec. III in SI for the protocols for preparing the packings), and all the simulations are performed at the indent location right above the same surface particle in each packing. For comparison, all the curves in (a)–(d) have the same maximum indentation depth as that in Fig. 1b, which is 9.27 nm. Note the greatly reduced load scale in (c) and (d).

The simulation results in Fig. 5 also demonstrate that friction and adhesion synergistically stabilize and toughen the DNPs to a great extent. Note that friction itself is able to endow only limited mechanical strength in the case of weak adhesion ( $w = 0.1 \ w_0$ , Fig. 5c). Higher friction

yields somewhat higher strength, but is still far less effective at strengthening a DNP than tightened by the adhesive force (Fig. 5a). We ascertain that the indentation load drops shown in Fig. 5c correspond to structural instabilities resulting in pile-up on the packings' surface due to the shear dilatancy effect induced by the indentation (see Supporting Movie S3). This effect is suppressed when adhesion is enhanced (Fig. 5a and Supporting Movie S1), since the adhesive force makes dilatancy harder.

The adhesive but frictionless packings (Fig. 5d) do gain enhanced stiffness in the case of stronger adhesion; however, they remain structurally unstable as evidenced by the precipitous serrations on the load curves. Each serration corresponds to softening or breaking of one or more interparticle bonds (Supporting Movie S4), which is attributed to the external force separating two particles exceeding their pull-off force, i.e., the negative of the minimum of the normal elastic contact force between them. Consequently, it will suddenly break the force balance of the global normal contact force chains, which may lead to a structural rearrangement. Generally, higher *w* results in a larger pull-off force and a larger rearrangement, which limits the attainable mechanical strength of the packings with strong adhesion but no friction.

However, this situation can be significantly alleviated by introducing friction (Fig. 5b), since friction offers shearing resistance and effectively mitigates particle rearrangements, thus improving toughness. As well, stronger adhesion strengthens the frictional forces. Unlike in an atomic glass, in which the interatomic potential energy released by atomic rearrangements is converted into kinetic energy, in a DNP the interparticle potential energy of normal contact released during plastic deformation is mainly dissipated by friction rather than particle vibrations (see Fig. S12 in SI). In this regard, friction enhances the ability of the packing to absorb energy and hinders further exploration in configurational space to relax strain energy. This also suggests interparticle friction as a mechanism for improving the mechanical stability and toughness of disordered materials. Moreover, the adhesive force can be strengthened by shortening the interparticle separation with the aid of the tangential frictional force, which retards the de-bonding of particles and thus further enhances toughness. The interplay of friction and adhesion revealed here suggests possibly establishing a more general jamming phase diagram, which could incorporate those for frictional particles<sup>25</sup> and for attractive particles<sup>39,59,60</sup>, generalizing Liu and Nagel's original jamming phase diagram<sup>61</sup>.

# IV. CONCLUSION

We have developed the MADEM approach, which can handle packings consisting of polydisperse frictional and adhesive particles undergoing large deformation. MADEM can straightforwardly deal with macroscopic granular systems by simply ignoring the interparticle adhesion, and can also be conveniently extended to simulate colloidal systems by applying additional Stokes' drag force and stochastic force on particles.

We have modeled recent unique indentation experiments conducted on DNPs with single nanoparticle resolution. By performing MADEM simulations, we have reproduced multiple attributes of the DNPs that match previous experiments. This includes substantial particle-level spatial heterogeneity in stiffness, energy dissipation, and the amount of plasticity. This agreement is attained when using a value of adhesion several times greater than the van der Waals adhesion value for the nanoparticles, suggesting that stronger bonding mechanisms such as covalent bonds, hydrogen bonds, or capillary forces<sup>12</sup> were present in the experiments. We have also shown that thermal activation can be omitted in our DNPs wherein strong dissipation exists, despite the fact that the constituent particles are nanoscale in size.

Furthermore, we uncover the mechanisms of the localized yielding and hardening phenomena observed in both experiments and simulations, where switching of the interparticle bonding plays a critical role. This demonstrates that signatures of plasticity in this system, and perhaps others, can involve changes in the magnitude and sign of interparticle interaction forces in the absence of particle rearrangements. This adds a new dimension to the theory of how plasticity initiates in disordered systems. We further demonstrate a strong interplay between friction and adhesion is crucial to retard plastic deformation and give rise to enhanced structural stability and toughness of the DNPs. This deepens the understanding of the roles of friction and adhesion in regulating the deformation of DNPs, and may furnish possible guidance for designing DNPs with better mechanical performance.

This work helps to establish connections between the physics of DNPs and other amorphous systems. For example, atomic glasses with covalent bonding may feature similarly enhanced stiffness compared to more isotropically bonded system, since the directional nature of covalent bonds provides an angular resistance, which bears a certain resemblance to interparticle friction. Any atomic glass, regardless of bonding type, is expected to behave similarly in some aspects to

DNPs, as attractive forces are present in both cases. Moreover, DNPs should share similar behavior with many geological systems<sup>62</sup>, where friction and adhesion are of key importance as well, such as the pressure sensitivity and flow non-normality in the yield surface<sup>63,64</sup>. For instance, the strong dependence of the indentation load on adhesion in the presence of friction that we report (Fig. 5b) is indicative of the pressure sensitivity of the yielding, since adhesion acts like a confining pressure in jamming systems<sup>39</sup>. In general, the current simulations provide a means by which the similarities and differences between atomic glasses and larger-scale granular matter may be explored, in particular by varying the bonding potential, mass, and length scale.

## SUPPORTING INFORMATION

Introduction of the MADEM we develop; Error analysis of the adhesive force between a coated sphere and a semi-infinite plane; Protocols for preparing nanoparticle packings for indentation simulations and packing fraction calculation; Effect of the work of adhesion on packing fraction; Effect of the indenter size on mechanical response; Effect of the indentation velocity on mechanical response; A supporting table listing the formulas for the energy calculation listed in Fig. 3; A supporting figure displaying the evolution of the power of the normal elastic energy and the sliding plastic energy for the curve with  $\mu_s = 0.3$  and  $w = 7w_0$  shown in Fig. 5; Four supporting movies showing the evolution of the packing configuration over the course of the indentation corresponding to Fig. 1, the evolution of the interparticle normal contact force chains and the sliding frictional force chains corresponding to Fig. 4, the evolution of the packing configuration with  $\mu_s = 0.3$  and  $w = 0.1w_0$ , and the evolution of the interparticle normal contact force chains of the packing with  $\mu_s = 0$  and  $w = 7w_0$ , respectively.

## **ACKNOWLEDGEMENTS**

X.L. acknowledges support by the China Scholarship Council (201406235041), and thanks helpful discussions with Dr. Wenbin Li and Dr. Yunwei Mao. J.A.L. acknowledges support from the Ashton Foundation. R.W.C. acknowledges support from the UPENN MRSEC, NSF DMR-1720530, as well as partial support from NSF DMR-1120901. J.L. acknowledges support by NSF DMR-1923976. This work was carried out in part at the Singh Center for Nanotechnology, which

is supported by the NSF National Nanotechnology Coordinated Infrastructure Program under grant NNCI-2025608.

#### REFERENCES

- (1) Royer, J. R.; Chaikin, P. M. *PNAS* **2015**, 112, 49-53.
- (2) Kou, B.; Cao, Y.; Li, J.; Xia, C.; Li, Z.; Dong, H.; Zhang, A.; Zhang, J.; Kob, W.; Wang, Y. *Nature* **2017**, 551, 360-363.
- (3) Xing, Y.; Zheng, J.; Li, J.; Cao, Y.; Pan, W.; Zhang, J.; Wang, Y. Phys. Rev. Lett. 2021, 126, 048002.
- (4) Cubuk, E. D.; Schoenholz, S. S.; Rieser, J. M.; Malone, B. D.; Rottler, J.; Durian, D. J.; Kaxiras, E.; Liu, A. J. *Phys. Rev. Lett.* **2015**, 114, 108001.
- (5) Li, W.; Rieser, J. M.; Liu, A. J.; Durian, D. J.; Li, J. *Phys. Rev. E* **2015**, 91, 062212.
- (6) Rieser, J. M.; Arratia, P. E.; Yodh, A. G.; Gollub, J. P.; Durian, D. J. Langmuir 2015, 31, 2421-2429.
- (7) Utter, B.; Behringer, R. Phys. Rev. Lett. 2008, 100, 208302.
- (8) Wang, Y.; Wang, Y.; Zhang, J. *Nature Commun.* **2020**, 11, 4349.
- (9) Zhang, L.; Prosser, J. H.; Feng, G.; Lee, D. *Nanoscale* **2012**, 4, 6543-52.
- (10) Zhang, L.; Feng, G.; Zeravcic, Z.; Brugarolas, T.; Liu, A. J.; Lee, D. ACS Nano 2013, 7, 8043-8050.
- (11) Lefever, J. A.; Jacobs, T. D.; Tam, Q.; Hor, J. L.; Huang, Y.-R.; Lee, D.; Carpick, R. W. *Nano Lett.* **2016**, 16, 2455-2462.
- (12) Lefever, J. A.; Mulderrig, J. P.; Hor, J. L.; Lee, D.; Carpick, R. W. Nano Lett. 2018, 18, 5418-5425.
- (13) An, L.; Zhang, D.; Zhang, L.; Feng, G. Nanoscale 2019, 11, 9563-9573.
- (14) Cubuk, E. D.; Ivancic, R. J. S.; Schoenholz, S. S.; Strickland, D. J.; Basu, A.; Davidson, Z. S.; Fontaine, J.; Hor, J. L.; Huang, Y. R.; Jiang, Y.; Keim, N. C.; Koshigan, K. D.; Lefever, J. A.; Liu, T.; Ma, X. G.; Magagnosc, D. J.; Morrow, E.; Ortiz, C. P.; Rieser, J. M.; Shavit, A.; Still, T.; Xu, Y.; Zhang, Y.; Nordstrom, K. N.; Arratia, P. E.; Carpick, R. W.; Durian, D. J.; Fakhraai, Z.; Jerolmack, D. J.; Lee, D.; Li, J.; Riggleman, R.; Turner, K. T.; Yodh, A. G.; Gianola, D. S.; Liu, A. J. *Science* 2017, 358, 1033-1037.
- (15) Jang, D.; Greer, J. R. Nature Mater. 2010, 9, 215-219.
- (16) Jang, D.; Gross, C. T.; Greer, J. R. Int. J. Plast. **2011**, 27, 858-867.
- (17) Greer, A. L.; Cheng, Y. Q.; Ma, E. *Mater. Sci. Eng.*, R **2013**, 74, 71-132.
- (18) Ding, B.; Li, X.; Zhang, X.; Wu, H.; Xu, Z.; Gao, H. Nano Energy 2015, 18, 89-96.
- (19) Zhou, X.; Zhou, H.; Li, X.; Chen, C. J. Mech. Phys. Solids 2015, 84, 130-144.
- (20) Schall, P.; Weitz, D. A.; Spaepen, F. Science 2007, 318, 1895-1899.
- (21) Strickland, D. J.; Huang, Y.-R.; Lee, D.; Gianola, D. S. PNAS 2014, 111, 18167-18172.
- (22) Richard, D.; Ozawa, M.; Patinet, S.; Stanifer, E.; Shang, B.; Ridout, S. A.; Xu, B.; Zhang, G.; Morse, P. K.; Barrat, J. L.; Berthier, L.; Falk, M. L.; Guan, P.; Liu, A. J.; Martens, K.; Sastry, S.; Vandembroucq, D.; Lerner, E.; Manning, M. L. *Phys. Rev. Mater.* **2020**, 4, 113609.
- (23) Argon, A. S. Acta Metall. 1979, 27, 47-58.
- (24) Scott, G. D. Nature 1960, 188, 908.
- (25) Bi, D.; Zhang, J.; Chakraborty, B.; Behringer, R. P. Nature 2011, 480, 355-8.
- (26) Singh, A.; Ness, C.; Seto, R.; de Pablo, J. J.; Jaeger, H. M. Phys. Rev. Lett. 2020, 124, 248005.
- (27) Mo, Y.; Turner, K. T.; Szlufarska, I. *Nature* **2009**, 457, 1116-1119.
- (28) Mate, C. M.; Carpick, R. W., *Tribology on the Small Scale: A Modern Textbook on Friction, Lubrication, and Wear.* OUP Oxford: 2019.
- (29) Lee, D.; Rubner, M. F.; Cohen, R. E. Nano Lett. 2006, 6, 2305-2312.
- (30) Wu, Z.; Lee, D.; Rubner, M. F.; Cohen, R. E. Small (Weinheim an der Bergstrasse, Germany) 2007, 3, 1445-1451.
- (31) Park, K.; Seo, D.; Lee, J. Colloids Surf., A 2008, 313, 351-354.

- (32) Cook, K. T.; Tettey, K. E.; Bunch, R. M.; Lee, D.; Nolte, A. J. ACS Appl. Mat. Interfaces 2012, 4, 6426-6431.
- (33) Huang, Y.-R.; Park, J. T.; Prosser, J. H.; Kim, J. H.; Lee, D. *Journal of Materials Chemistry C* **2014**, 2, 3260-3269.
- (34) Park, J. T.; Kim, J. H.; Lee, D. *Nanoscale* **2014**, 6, 7362-7368.
- (35) Tan, S.; Hashim, H.; Lee, C.; Taib, M. R.; Yan, J. Energy procedia 2014, 61, 704-708.
- (36) Soliveri, G.; Ardizzone, S.; Yüksel, S.; Cialla-May, D.; Popp, J.; Schubert, U. S.; Hoeppener, S. *J. Phys. Chem. C* **2016**, 120, 1237-1244.
- (37) Stein, P.; Moradabadi, A.; Diehm, M.; Xu, B.-X.; Albe, K. Acta Mater. 2018, 159, 225-240.
- (38) Jiang, Y.; Hor, J. L.; Lee, D.; Turner, K. T. ACS Appl. Mat. Interfaces 2018, 10, 44011-44017.
- (39) Trappe, V.; Prasad, V.; Cipelletti, L.; Segre, P. N.; Weitz, D. A. Nature 2001, 411, 772-775.
- (40) Lois, G.; Blawzdziewicz, J.; O'Hern, C. S. Phys. Rev. Lett. 2008, 100, 028001.
- (41) Martin, C. L.; Bordia, R. K. Phys. Rev. E 2008, 77, 031307.
- (42) Parteli, E. J.; Schmidt, J.; Blümel, C.; Wirth, K.-E.; Peukert, W.; Pöschel, T. Sci. Rep. 2014, 4, 6227.
- (43) Liu, W.; Li, S.; Baule, A.; Makse, H. A. Soft Matter 2015, 11, 6492-6498.
- (44) Ma, X.; Liu, J.; Zhang, Y.; Habdas, P.; Yodh, A. J. Chem. Phys. 2019, 150, 144907.
- (45) Munjiza, A. A., The combined finite-discrete element method. John Wiley & Sons: 2004.
- (46) Sauer, R. A.; Li, S. Int. J. Numer. Methods Eng. 2007, 71, 931-962.
- (47) Luding, S. Granular Matter 2008, 10, 235-246.
- (48) Li, S.; Marshall, J. S.; Liu, G.; Yao, Q. Prog. Energy Combust. Sci. 2011, 37, 633-668.
- (49) Thornton, C.; Cummins, S. J.; Cleary, P. W. Powder Technol. 2013, 233, 30-46.
- (50) Marshall, J. S.; Li, S., Adhesive particle flow. Cambridge University Press: 2014.
- (51) Plimpton, S. J. Comput. Phys. 1995, 117, 1-19.
- (52) Israelachvili, J. N., Intermolecular and surface forces. Elsevier Science: 2011.
- (53) Shimizu, F.; Ogata, S.; Li, J. Mater. Trans. 2007, 48, 2923-2927.
- (54) Li, J. Modell. Simul. Mater. Sci. Eng. 2003, 11, 173.
- (55) Goldenberg, C.; Goldhirsch, I. Nature 2005, 435, 188.
- (56) Oliver, W. C.; Pharr, G. M. J. Mater. Res. 1992, 7, 1564-1583.
- (57) Rottler, J.; Schoenholz, S. S.; Liu, A. J. Phys. Rev. E 2014, 89, 042304.
- (58) Patinet, S.; Vandembroucq, D.; Falk, M. L. Phys. Rev. Lett. 2016, 117, 045501.
- (59) Sadati, M.; Taheri Qazvini, N.; Krishnan, R.; Park, C. Y.; Fredberg, J. J. Differentiation 2013, 86, 121-125.
- (60) Zheng, W.; Liu, H.; Xu, N. Phys. Rev. E 2016, 94, 062608.
- (61) Liu, A. J.; Nagel, S. R. Nature 1998, 396, 21-22.
- (62) Das, B. M.; Sobhan, K., Principles of Geotechnical Engineering. Cengage Learning: 2013.
- (63) Gao, Y. F.; Wang, L.; Bei, H.; Nieh, T. G. Acta Mater. 2011, 59, 4159-4167.
- (64) Rudnicki, J. W.; Rice, J. R. J. Mech. Phys. Solids 1975, 23, 371-394.